From the (1B) Spectroscopic State to the Photochemical Product of the Ultrafast Ring-Opening of 1,3-Cyclohexadiene

THE JOURNAL OF PHYSICAL CHEMISTRY A

Article

pubs.acs.org/JPCA

From the (1B) Spectroscopic State to the Photochemical Product of the Ultrafast Ring-Opening of 1,3-Cyclohexadiene: A Spectral Observation of the Complete Reaction Path

Christine C. Pemberton,[†] Yao Zhang,[†] Kenichiro Saita,[‡] Adam Kirrander,[‡] and Peter M. Weber*[,†]

[†]Department of Chemistry, Brown University, Providence, Rhode Island 02912, United States

[‡]EaStCHEM, School of Chemistry, University of Edinburgh, Edinburgh EH9 3FJ, United Kingdom

ABSTRACT: All stages of the electrocyclic ring-opening of 1,3-cyclohexadiene (CHD) were observed by time-resolved photoionization-photoelectron spectroscopy. Spectra of the 1B state, previously unobserved using time-resolved methods, were obtained upon optical excitation using ultrashort laser pulses at 4.60 or 4.65 eV, followed by ionization with pulses at 3.81, 3.85, and 4.10 eV, revealing a 1B lifetime of 30 fs. In an experiment using 3.07 eV probe photons and a 4.69 eV pump, we observed a time-sequenced progression of Rydberg states that includes s, p, and d states of the series n = 3 to 6. The sequentiality of the Rydberg signals points to an ionization mechanism that captures the molecule on different points along the reaction path in 2A. A dynamic fit of the Rydberg signals, coupled with MS-CASPT2 calculations, reveals that as the wavepacket moves down the potential energy surface it acquires kinetic energy at a rate of 28 eV/ps before reaching the conical intersection to the 1A ground state. During the reaction, the terminal carbon atoms separate at a speed of 16 Å/ps. A deconvolution of the Rydberg signals from a broad feature assigned to structurally disperse 1,3,5-hexatriene (HT) shows the formation of the open-chain hexatriene structure with an onset 142 fs after the initial absorption of a pump photon. The experimental observations are discussed in the context of recent ultrafast X-ray scattering experiments and theoretical quantum dynamics simulations.

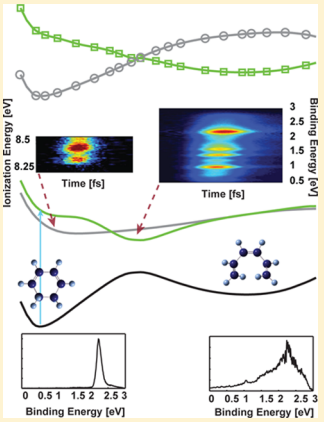

INTRODUCTION

The ring-opening of 1,3-cyclohexadiene (CHD) serves as a model for understanding photochemical electrocyclic reactions. With myriad occurrences and applications, such as its involvement in the synthesis of vitamin D,[1,2] the design of photochemical switches,[3] and its general importance to synthetic organic chemistry,[4] the reaction has been widely investigated. The reaction path is thought to be as the follows: Absorption of UV light in the range of 4.4 to 5.9 eV lifts the molecule into the first excited state of 1B symmetry.[7,10] From there, the wavepacket quickly accelerates toward a conical intersection, which it bypasses as it transitions to the doubly excited 2A state. It is that state that correlates with the ground state of the reaction product, 1,3,5-hexatriene (HT) and hence enables the ring-opening in accordance with the Woodward–Hoffmann rules.[5,6] A symmetry breaking motion away from the minimum energy path guides the wavepacket to a conical intersection between the 2A and 1A electronic surfaces,[7−9] which facilitates the decay to the electronic ground state of the reaction product.

Starting with the studies of van der Lugt and Oosterhoff,[10] our present understanding of this reaction rests on a combination of experimental and computational investigations.[6−9,11−17] Experimentally, the reaction path is difficult to map because it proceeds so quickly and because suitable spectroscopies are lacking. As summarized in a recent review,[18] many experimental studies have been performed, both in condensed phases[19−24] and in the gas phase or in molecular beams,[25,7,27,28,26] but they do not always give consistent results. From the point of view of theory, computations remain challenging because of the difficulty in calculating doubly excited states and conical intersections accurately, and the fundamental computational limitations imposed on quantum dynamics in low symmetry systems with many degrees of freedom.

The ring-opening reaction of CHD poses particular challenges to time-resolved experiments because the involved electronic states are difficult to probe and the time scales are very short. Successful experiments have taken advantage of ionization with low photon energy, high intensity probe pulses to explore the time scales of the reaction process.[7,27] These probe pulses ionize the time-evolving molecules in a multiphoton process that generates ions of various energy content, which leads to fragmentation patterns that are deemed to be characteristic of molecular species at the time of ionization: as the wavepacket travels down the steep potential it acquires vibrational energy, which, upon ionization, causes the fragmentation. Consequently, the relative intensities of individual fragments change in time. The interpretation of these experiments is based on the premise that the fragmentation patterns are uniquely associated with the specific electronic states populated during the reaction. Through these

Received: June 14, 2015
Revised: July 17, 2015
Published: July 20, 2015

DOI: 10.1021/acs.jpca.5b05672
J. Phys. Chem. A 2015, 119, 8832−8845

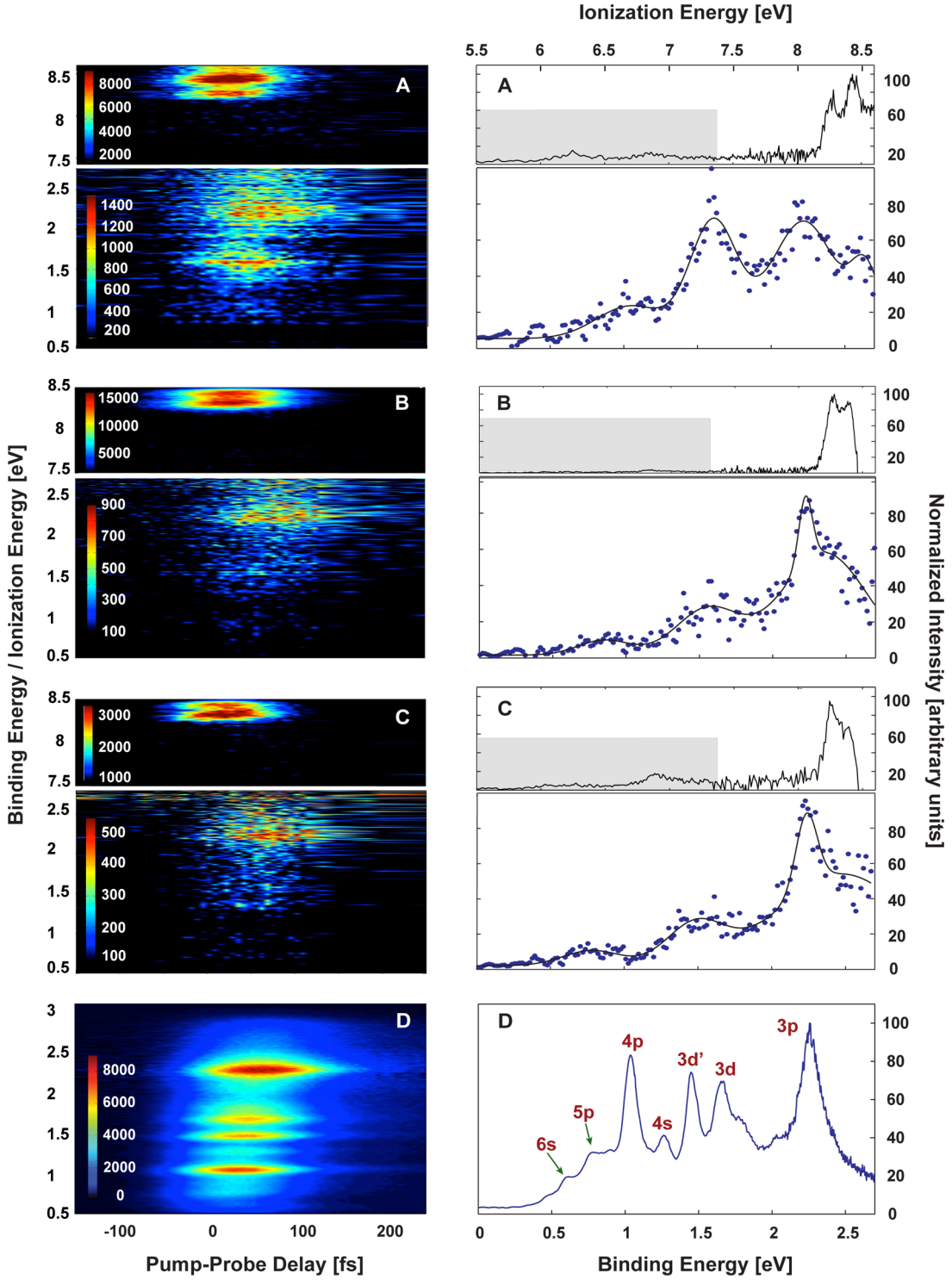

Figure 1. Time-resolved photoelectron spectra of CHD, left column, and projection onto the energy axis, right column. Pump/probe photon energies are as follows: (A) 4.65 eV/4.10 eV; (B) 4.60 eV/3.85 eV; (C) 4.65 eV/3.81 eV; (D) 4.69 eV/3.07 eV. In the contour plots the color encodes the intensity on a linear scale. Each subfigure in panels A−C is composed as follows: Top: Spectral region of the 1B state (BE = 3.5 − 4.0 eV; IE = 8 − 8.5 eV), Bottom: Rydberg state region (BE = 0.5 − 2.5 eV). In the contourplots, the energy axis on the left plots the binding energy for the subfigures on the bottom, and panel D. The subfigures on top are plotted against the ionization energy. In the energy projection, the subfigures on top are to be read with the axis on the top (ionization energy), the subfigures on the bottom are to be read with the axis on the bottom (binding energy). In the energy projection plots, the spectra on the bottom of each subplot represent the ranges shaded in gray in the top graphs. The blue circles in the Rydberg spectra represent the experimental data, the black solid lines depict the fits as described in the text. In the contour plots, the intensity-axis has been adjusted to enhance the visibility of the signals in each region.

time-dependent ion signals, lifetimes of 53−56 and 77−80 fs were found for the 1B and 2A states, respectively.[7,27]

Photoelectron spectroscopy, which can be implemented in a pump−probe scheme just like mass spectrometry, can provide

DOI: 10.1021/acs.jpca.5b05672
J. Phys. Chem. A 2015, 119, 8832−8845

additional information about the molecular reaction pathways. The time-resolved CHD spectra of Kuthrimmal et al.[28] showed a progression of Rydberg peaks with a 55 fs rise and a decay of 84 fs. To explain the observed Rydberg peaks, Kuthirummal et al. invoked a transition to a superexcited state that quickly reacts to the Rydberg levels, a mechanism that has been found in other molecular systems.[29−31] While details of the ionization mechanism remained speculative, the existence of a rise time, as well as the agreement of the time scales, suggested that the time profile of the Rydberg states represents the temporal evolution of the 2A state.[28] A recent photoelectron spectroscopic study explored the formation of HT and reformation of CHD in the electronic ground state after photo excitation and subsequent relaxation.[32] That investigation probed the lifetimes of 1B and 2A via direct ionization using 13.6 eV probe photons. Time constants of 70 and 60 fs for 1B and 2A, respectively, are in reasonable agreement with the prior studies.

In spite of the tremendous advances embodied by these studies, many mysteries of the ring-opening reaction of CHD remain to be explored. Specifically, it is curious that all the Rydberg peaks observed in the photoelectron spectra of Kuthirummal et al. seemed to appear in unison. As the molecular structure evolves rapidly along the reaction path, one would expect the photoelectron spectra to evolve as well, that is, the individual Rydberg peaks should exhibit distinct time dependencies. Without a change in the spectral signature that would indicate an evolution of structure or the formation of the product, it is not even clear if the mass spectrometry or photoelectron spectroscopy experiments indeed captured the dominant part of the wavepacket as it moves toward HT, or possibly just a part of it that is most easily ionized.[7] Similarly, one might wonder if the delayed rise in the Rydberg signal, interpreted as representing the rise of the 2A state, instead relates to the time the wavepacket spends traveling along the S_1 electronic surfaces before a resonance with the postulated superexcited state is reached.

In the present study, taken with improved time resolution and tunable lasers, spectral signatures are attained for every step along the electrolytic ring-opening of CHD. As in the prior studies, we initiate the reaction by exciting CHD to the 1B state using an ultrashort laser pulse at 265 nm. To elucidate the ionization process we ionize the molecules during the reaction with variable wavelength probe pulses in the range of 404 to 300 nm. The different probe pulse wavelengths lead to systematic variations in the photoelectron spectra, which enables us to gain a deeper understanding of the reaction path and the ionization mechanism. Importantly, we were able to directly observe the time dependence of the 1B state and to uncover a sequentiality of the Rydberg peaks as the reaction unfolds. This allows us to identify the ionization pathway and thereby deduce the correlation of the vibrational energy of the ion in its final state with the progress of the reaction path. A combination with computational results then enables us to quantitatively map the path of the dynamical reaction as it unfolds in CHD. Importantly, several long-held assumptions about the ionization process are revised as we gain a deeper insight into the reaction mechanism.

The spectroscopic view of the ring-opening reaction of CHD presented here should be compared to the structural view afforded by the X-ray diffraction experiments that we conducted recently using ultrafast, high intensity X-ray pulses from the LCLS free electron laser at the SLAC National Accelerator Laboratory.[33,34] The structural study reveals the atomic motions as the reaction proceeds, thereby giving a picture of a chemical reaction that accords with chemical intuition, while the spectroscopic results presented here offer deeper insights into the involved electronic states. In principle, it should also be possible to invert the Rydberg level binding energies that we measure here to derive a time-dependent molecular structure.[35,36] However, the computation of binding energies of Rydberg levels converging to the possibly core-excited and highly distorted HT ion, as would be necessary to deduce the structures from the photoelectron experiments, remains challenging for the CHD system.

EXPERIMENTAL METHODS

A molecular beam was created by flowing helium at 1.5 bar through liquid 1,3-cyclohexadiene (Aldrich, 97%) and expanding the vapor through a 100 μm nozzle orifice and a skimmer. For data presented in panels A through C in Figure 1 the diameter of the skimmer orifice was 170 μm. For the experiments shown in panel D, a 210 μm skimmer was used. The liquid sample was cooled to below −30 °C in order to avoid the formation of van der Waals clusters. The molecular beam is crossed perpendicularly by ultrafast laser pulses that are generated by a chirped pulse amplifier with an additional single pass amplifier between the regenerative amplifier and the compressor (Legend Elite Duo, Coherent). The amplifier was seeded by a Ti:sapphire laser (Mantis, Coherent) and pumped by two 5 kHz Nd:YLF lasers (Evolution 30, Coherent, Regenerative Amplifier; Evolution HE, Coherent, Single Pass Crystal). The near-IR fundamental output of the amplifier system, about 12 W at a repetition rate of 5 kHz, was divided by a 90% beam splitter into two parts.

For the pump−probe experiments exploring the time sequence of the Rydberg states, the smaller portion (∼1 W) is focused by a curved mirror into a 0.1 mm thick BBO type I crystal, yielding the second harmonic ($\hbar\omega_2$, 404 nm, 3.07 eV) probe pulses with a fwhm of 5.4 nm (46 meV). The larger part of the beam (∼11 W) was directed into an optical parametric amplifier (Opera Solo, Coherent), where a pump pulse was generated at a wavelength of 265 nm (4.69 eV) and a bandwidth of 3.7 nm (70 meV). Pulse energies were 4 μJ for the pump and 9 μJ for the probe pulses, respectively.

For the experiments probing the dynamics of the 1B state, pump and probe were reversed. A 0.3 mm thick BBO type II crystal was placed immediately behind the type I crystal, yielding the third harmonic pump pulse. Due to slight shifts in the center wavelength and spectral profile of the Ti:sapphire laser seeding the regenerative amplifier, the center wavelengths of the third harmonic pump pulses varied slightly between experimental runs, leading to $\hbar\omega_3$ = 266 nm (4.65 eV) and $\hbar\omega_3$ = 269 nm (4.60 eV), with fwhm of 1.7 nm (30 meV) and 3.7 nm (63 meV), respectively. The optical parametric amplifier was used to generate probe pulses at wavelengths of 300 nm (4.10 eV), 322 nm (3.85 eV), and 325 nm (3.81 eV) with bandwidths of 50, 52, and 51 meV, respectively. Pulse energies were about 1 μJ for the pump pulses, and 1, 5, and 4 μJ, respectively, for the 4.10, 3.85, and 3.81 eV probe pulses. No evidence of effects of laser polarization where found.[48]

Both the pump and the probe beams were focused into the interaction region by a curved mirror (f = 500 mm). Intensities of the focused pump pulses were estimated to be between 3×10^{11} W/cm^2 (Figure 1D) and 4×10^{12} W/cm^2 (Figure 1A−C). Probe intensities were 2×10^{11} W/cm^2 (4.10 eV probe), 7×10^{11} W/cm^2 (3.85 eV probe), 8×10^{11} W/cm^2 (3.81 eV

DOI: 10.1021/acs.jpca.5b05672
J. Phys. Chem. A 2015, 119, 8832−8845

probe), and 2 × 10^{13} W/cm^2 (3.07 eV probe), respectively. These intensities were calculated assuming Gaussian beam optics, but spherical aberration likely causes the true focal spot sizes to be larger so that these intensities should be viewed as upper limits.

Photoelectrons were collected and recorded by a time-of-flight photoelectron spectrometer that has been described in detail elsewhere.[37−40] To calibrate the time-resolved photoelectron spectra and determine time zero, we used photoionization of acetone. A Gaussian fit of the temporal evolution of the acetone parent ion determined the full width at half maximum of the instrument function to values between 99 and 103 fs in all experiments.

To avoid drift in time zero between experimental runs, the CHD and acetone ion signals were collected together in a calibration run. A careful comparison of the total ion signal of CHD with and without acetone confirmed that the presence of acetone does not affect the CHD signal. Since the total photoionization signals of electrons and ions have to coincide in time, comparing the temporal evolution of the total ion signal of CHD with the total photoelectron signal was used to measure time zero in the photoelectron spectra.

COMPUTATIONAL METHODS

The minimum potential energy path on the 1^1B state was computed by the three-state averaged complete active space self-consistent field (SA3-CASSCF) method[41,42] using the cc-pVDZ (correlation-consistent polarized valence double-ζ) basis set[43] and the MOLPRO 2012.1 quantum chemistry package.[44] The active space consisted of four orbitals with six electrons, CAS(6,4), for the neutral species. In the geometry optimization, the molecular geometry was restricted under the C_2 symmetry, but the electronic structure calculations were performed without use of symmetry. The potential energies were corrected at the multistate multireference complete active space second-order perturbation theory (MS-MR-CASPT2) level,[45,46] and a level shift of 0.2 hartree was used in the MS-CASPT2 calculation. The 1^2A and 1^2B potential energies of the ionized species were also computed at the MS-MR-CASPT2/cc-pVDZ level. In this part, the molecular geometry was the same as the one on the 1^1B minimum energy path and the wave function was determined by the SA2-CAS(5,4)-SCF calculation.

RESULTS AND DISCUSSION

Figure 1, left column, shows CHD's time-resolved photoelectron spectra, where the electron binding energy is plotted as a function of the pump−probe time delay. The spectra were obtained upon multiphoton ionization with different combinations of 4.6−4.7 eV pump photons and 3−4 eV probe photons as given in the figure caption. The one-color background signals were subtracted so that only the two-color ionization signals are shown. The right column of Figure 1 shows projections of the time-dependent spectra onto the energy axis.

While the directly measured observable is the kinetic energy of the photoelectrons, the photoelectron spectra can be constructed in either of two ways. The binding energy is given by subtracting the measured photoelectron energy from the energy of just the ionizing probe photon. The ionization energy spectrum is obtained by subtracting the electron kinetic energy from the sum of all ionizing photon energies. While for the former one only needs to know the energy of the ionizing photon, for the latter one also needs to make assumptions about how many photons are involved in the ionization, a parameter that may be different for different parts of a spectrum. Both the ionization energy and the binding energy scales are provided in Figure 1, but one should keep in mind that the ionization energy of CHD is 8.25 eV, so that signals with apparent ionization energy less than that must stem from ionization mechanisms requiring more photons than assumed.

As explained in more detail below, the signal around the binding energy (BE) of 3.5 eV, most visible in panels A through C, arises from the one-photon pump pulse excitation to the 1B state and 1-photon probe pulse ionization. The time evolution of that signal represents the dynamics of the 1B state. The signals at BE = 0.5 to 2.5 eV, visible with different intensities in all panels, stem from the one-photon pump pulse excitation to 1B, followed by conversion into the 2A state. There, the dynamics evolved before the probe pulse lifts the molecule through a Rydberg state to the ion. The spectral signatures are those of the Rydberg states. The time-resolved photoelectron spectrum of panel D, which is taken with the highest intensity probe pulses, shows the Rydberg peaks most clearly. Using laser pulses of somewhat longer duration, and concomitantly smaller bandwidth, these peaks have previously been identified by Kuthirummal et al. as the s (δ = 0.93), p (δ = 0.76), and d (δ = 0.15) Rydberg series ranging from n = 3 to 6.[28,26] Two peaks, one at 1.03 eV and one at 2.26 eV, remained unassigned by Kuthirummal et al. as their quantum defects (n = 4, δ = 0.36 and n = 3, δ = 0.55) did not seem to fit with those of other peaks. In a later investigation of the pump−probe photoelectron spectrum where the pump photon matched the excitation energy of 3p from the ground state (6 eV), the 2.26 eV peak was identified as 3p.[26,47] For the signal at 1.03 eV, investigations using higher energy pump photons showed that the position of this peak in the spectrum is independent of the excitation energy.[48] This suggests that this peak is a Rydberg state as well.

We propose here that the 1.03 eV peak results from the 4p Rydberg state and revise the assignment of the peaks at 1.27 eV (previously 4p) and 1.45 eV (previously 4s).[48] In our new assignment, the peak at 1.27 eV stems from the 4s Rydberg state, while the signal at 1.45 eV represents a magnetic sublevel of the 3d state, complementing the 3d state at 1.67 eV. Since we cannot confidently assign the 3d peaks at 1.45 and 1.67 eV to certain sublevels (e.g., 3d_{z^2}, $d_{x^2-y^2}$ as found in an electron impact investigation of ground state CHD[47,49]), we will refer to these states as 3d′ and 3d, respectively.

Panels A−C, taken with shorter wavelength ionization pulses of weaker intensity, show the 1B signal above 3.5 eV strongly, but only few of the Rydberg states. We attribute the latter observation to the lower intensity of the OPA probe pulses compared to the second harmonic pulses used for panel D, suggesting that higher order processes are involved in the generation of the Rydberg progression. Even so, those spectra do show two short-lived peaks in the binding energy region from 0 to 3 eV. A decomposition of the spectra into Gaussians,[50] shown as solid lines in panels A to C, gives binding energies of 2.23 ± 0.01 and 1.55 ± 0.06 eV (errors given are the standard deviations of all three measurements). Comparison with the spectrum in panel D, as well as previous investigations,[26] suggests that the 2.23 eV peak is the 3p Rydberg state. The 1.55 eV peak is quite weak and in the general vicinity of the 3d states.

DOI: 10.1021/acs.jpca.5b05672
J. Phys. Chem. A 2015, 119, 8832−8845

To explore the time dependent molecular dynamics, Figure 2 shows the temporal profiles for 1B (the signal taken with a 3.85 eV probe was used as an example), select Rydberg states (6s, 4p, 3d, and 3p), and the hexatriene product discussed below, plotted alongside the instrument function.

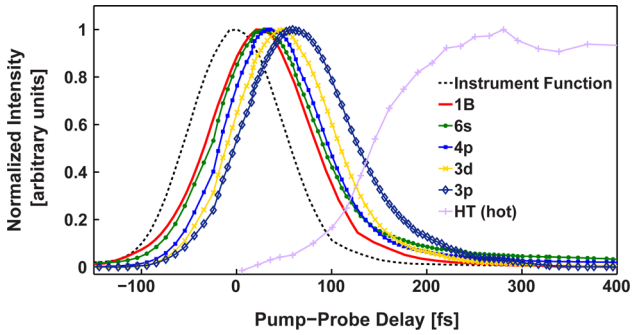

Figure 2. Temporal evolutions of 1B (pump, 4.65 eV; probe, 3.85 eV), select Rydberg states (6s, 4p, 3d, and 3p) and the product, HT (pump, 4.69 eV; probe, 3.07 eV), normalized to a maximum intensity of one and plotted against the instrument function (acetone ion signal; pump, 4.69 eV; probe, 3.07 eV).

The temporal profiles were obtained in the following manner: For the 1B state and the 6s and 4p Rydberg states, the signal for each peak was summed up in the energy domain around the peak maximum, over its fwhm. This gave the evolution of the intensity of each peak as a function of time. The time profiles for the Rydberg states, 3d and 3p, as well as the HT signal, were obtained via deconvolution of the Rydberg signals from a broad HT signature that arises after the disappearance of those Rydberg states. As described in ref 48, individual time traces of the 3p, 3d, and HT signatures were obtained by deconvoluting the spectrum at each time point in the energy domain. The time-dependent spectral weights represent the temporal evolutions of the corresponding species plotted in Figure 2. This experimental data is shown again in Figure 5 on a logarithmic intensity scale, along with dynamic fits.

1B State. Given CHD's vertical ionization energy of 8.25 eV,[51−55] and a 1B excitation energy of 4.65 eV (266 nm pump), single photon ionization out of 1B requires a probe photon energy of at least 3.6 eV. Consequently, only panels A through C of Figure 1 should be expected to show the direct ionization of 1B. We identify the strong signal at high binding energies (>3.5 eV) in these panels as the one-photon ionization of molecules initially excited to 1B. This interpretation is consistent with the measured binding energies, the early rise and short lifetimes of these signals, and their high intensity compared to later signals that arise from higher order processes (see below). This interpretation is also supported by the spectral signatures: plotting the photoelectron spectrum taken with the 4.10 eV probe pulses as a function of the ionization energy yields the spectrum of Figure 3A. This spectrum shows the same features as the well-known one-color, two-photon ionization spectrum at the pump wavelength,[28] Figure 3B. Consequently, this must be the spectral signature of the initially prepared 1B state. We note that this is the first spectral observation of 1B in a time-resolved experiment; all prior time-resolved experiments had insufficient time resolution and/or insufficient probe photon energy to measure the lifetime of the 1B state.

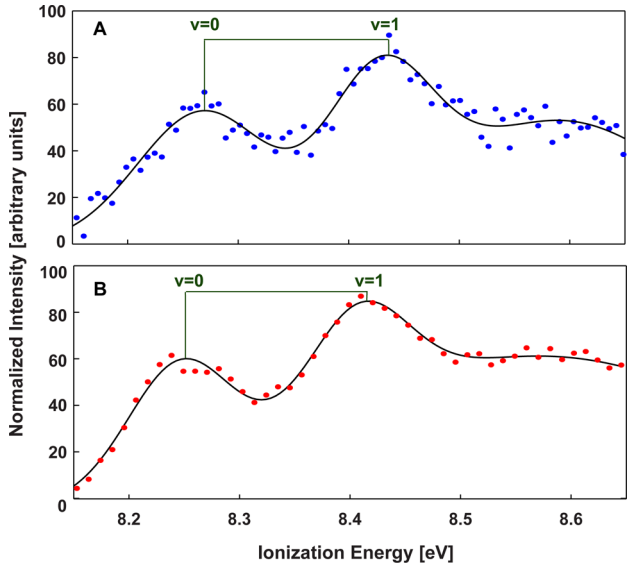

Figure 3. (A) Projection (sum over all time delays) of the two-color spectrum taken with a 4.65 eV pump and 4.10 eV probe onto the ionization energy coordinate. (B) One-color, two-photon ionization spectrum using just the 4.65 eV pump beam. The circles denote the experimental data, and the solid black lines represent fits to Gaussians.

The spectrum of Figure 3B shows two broad peaks (8.25 and 8.43 eV). The two-color spectrum, Figure 3A, integrates over all time delays and appears to show the peaks at slightly higher energy (0.01 eV). In the time delayed spectrum we observed a slight tilt (~300 meV/ps) toward higher ionization energies, which accounts for this difference. The 0.18 eV (1450 cm^{-1}) spacing between the peaks, close to the value reported previously,[28] has been interpreted as a vibrational progression of a C═C stretching vibration that is excited in the first step of the two-photon ionization, i.e., the preparation of CHD in the 1B state. It arises because the excitation from the 1A ground state to the 1B excited state weakens the double bonds of CHD. The same vibration was observed at 1578 cm^{-1} in the electronic ground state via Raman spectroscopy of the hot vapor by Autrey et al.[56] as well as in the gas-phase UV absorption spectrum by Garavelli et al.[7] The large widths of the peaks, 0.1 and 0.2 eV, respectively, result from progressions of 199 and 292 cm^{-1} ring twisting and ring puckering vibrations,[28,47] the individual spectral signatures of which cannot be discerned in the ultrafast time-resolved experiment. These vibrations are induced during the ionization transition.[28]

The time profiles of the observed 1B signals are shown in Figure 4. The solid lines are fits to single exponential decays convoluted with a Gaussian instrument function of 100 fs. Within the experimental uncertainty, the fits give a 1B decay time of 30 ± 2 fs. As we will show below, this value is consistent with the analysis of the Rydberg signals in Figure 1D, which does not show the 1B level directly because of the insufficient probe photon energy.

We note that the 30 ± 2 fs 1B decay time measured here is shorter than the previously reported time constant of 53 fs.[7,27,28] From an experimental side, it does appear possible that the interpretation of the time-resolved high-intensity mass spectra[7,27] might have been affected by assumptions about the reaction path that did not take into account the more complicated pathway that emerges from our present work. The photoelectron spectra previously measured by Kuthir-

DOI: 10.1021/acs.jpca.5b05672
J. Phys. Chem. A 2015, 119, 8832−8845

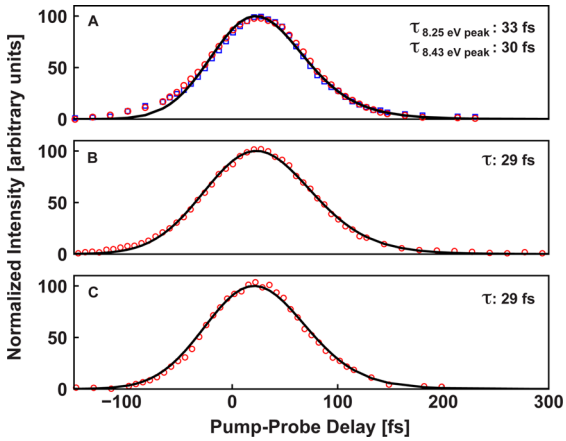

Figure 4. Time-resolved transients of the 1B state for the corresponding panels A through C of Figure 1. In panel A the red circles are for the vibrational peak at ionization energy of 8.25 eV, while the blue squares represent the peak at 8.43 eV.

ummal et al.[28] did not observe directly the disappearance of 1B. The time constant was instead inferred from the appearance of the Rydberg signals. Lacking the higher time resolution of the present experiment, Kuthirummal et al. combined all the Rydberg signals to analyze the time dependence. As we will show below, this procedure biases in favor of the most intense peaks, which turns out to be those that appear last in the sequence.

More fundamentally, the difference between the time constant measured here and those reported previously might be caused by the difference in coherence bandwidths of the excitation laser pulses. In the experiments reported here, the larger bandwidth supports a shorter laser pulse, but it also couples a wider range of molecular eigenstates, which therefore can support a faster decay of the 1B level. It is well-known that for transform limited optical pulses, the bandwidth of the excitation may alter the nature of the optically prepared state.[57,58] We point out that the time constant obtained here is more closely in agreement with the computations of Tamura et al., who found a decay time of 15−25 fs.[16] The 30 fs value is also in excellent agreement with new X-ray diffraction data and the associated computational studies. It therefore seems possible that the previously reported values were affected by the insufficiently coherent preparation of the 1B level and that the value found here more closely reflects the molecular lifetime of 1B.

At this point it is interesting to consider what dynamics takes place within the 1B state. In frequently used pictures, the 1B surface is depicted as steeply sloped in the Franck−Condon region but leading to an energy plateau further along the reaction coordinate.[7] One should therefore expect fast structural motions already within 1B toward a plateau that should be manifest in the time-dependent photoelectron spectra as a shift of the photoelectron peak energy with the delay time. While the photoelectron spectra do show a small shift, about 9 meV over the lifetime of the state, this shift is much smaller than one would expect from a rapidly evolving molecular structure. Additionally, as the molecule slides down the postulated steeply repulsive 1B surface, the energy required to reach the potential energy well of the molecular ion would increase with passing time. This means that the ionization with lower energy probe photons would cut off first, while higher energy probe photons would see the 1B state for a little longer, implying that the decay time of 1B would depend on the energy of the probe photon. Yet the analysis of the decay times (Figure 4) reveals no such effect. Combined, we conclude that we see no dynamics within the initially excited 1B level, an observation that would be consistent with the interpretation of the 1B lifetime as a decay of this initially excited state, or a dephasing of coherently excited molecular eigenstates as the molecule evolves from 1B to 2A.

Transition through the 2A State. The appearance of Rydberg spectral peaks that feature prominently in the time-resolved photoionization experiment with 3.07 eV photons (Figure 1D) was originally discovered by Kuthirummal et al.[28] Given the time resolution of their experiment, all Rydberg levels appeared to have the same time evolution. Yet even a cursory inspection of the more highly time-resolved spectra in Figures 1 and 2 shows that the different Rydberg states appear and disappear sequentially.

To explain the observation of the Rydberg states in the photoelectron spectrum, Kuthirummal et al. postulated that they are populated by an optical transition from the 2A state to a superexcited state, which in turn would decay to the Rydberg states within the duration of the probe pulses.[28] Ionization by a later part of the probe pulse would then reveal the Rydberg levels in the photoelectron spectrum. Given the time resolution of their study, and also given that even their probe pulse alone showed Rydberg state signatures that could only come about through such rapid relaxation mechanisms within the duration of the probe pulse, this explanation was rational. However, it is no longer consistent with the sequential temporal profiles seen in Figure 2. Instead, the sequentially appearing Rydberg signals must arise from a time-dependent transition probability between the 2A valence state and the individual Rydberg states as the wavepacket travels along the steeply sloped reaction path. This implies that the Rydberg levels are directly excited from the 2A surface.

To analyze the transient Rydberg peaks (Figure 5) we fit their time dependence using a dynamical model in which we assume that a coherent wavepacket travels along the reaction path and passes locations where the resonance transition between the 2A surface and individual Rydberg states matches the energy of the probe photon. This approach gave fits that

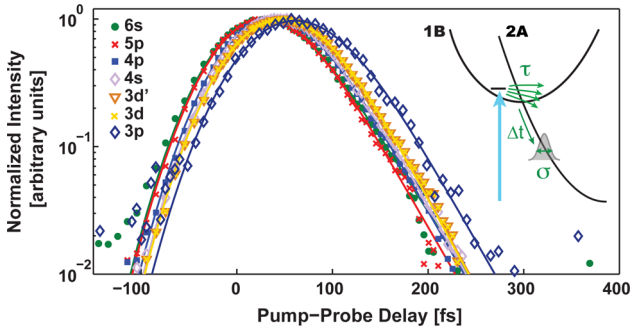

Figure 5. Rydberg peak transients observed in the experiment with 4.69 eV pump pulses and 3.07 eV probe pulses. Symbols represent experimental data as listed in the legend, and solid lines are the fits as described in the text. Inset: The model used for the dynamic fit. τ is the lifetime of 1B, and Δt is the time traveled along the reaction path before reaching the resonance window of width σ. Multiple arrows for τ illustrate the decay of the initially excited molecular state as the molecule evolves from 1B to 2A.

DOI: 10.1021/acs.jpca.5b05672
J. Phys. Chem. A 2015, 119, 8832−8845

were superior to one that assumed sequential kinetics with exponential rises and falls.

In the dynamic model, inset in Figure 5, the maximum transition probability corresponds to the optimal Franck–Condon overlap between the 2A state at a given location and a particular Rydberg state. The appearance and disappearance of a specific Rydberg signal depends on the time when the wavepacket reaches the location where the optical transition is in resonance, which we refer to as a "resonance window," and the speed with which the wavepacket traverses this window. The location of the resonance window is the one where the energy difference between the Rydberg state and the 2A state matches the photon energy. To model the time dependence of the Rydberg signals we describe the resonance windows by Gaussian functions in the time domain. As we will see, the fits reveal that most of the windows are open only for a very short duration, so that their exact functional form is probably of little consequence. As the exponential decay of the 1B state determines how many molecules enter the 2A state at any given time, the appearance and disappearance of the Rydberg signals is described by a convolution of the exponential decay with a Gaussian at variable center positions

$$I_{\mathrm{Ry}}(t) = \int_0^t \mathrm{d}t'\, \mathrm{e}^{-t'/\tau}\, \mathrm{e}^{-(t-t'-\Delta t)^2/2\sigma^2} \tag{1}$$

where τ is the lifetime of 1B, Δt is the time the wavepacket travels along the reaction path in 2A before reaching the center of the resonance window, and σ is the width (in time) of that window.

To fit the experimental data it was necessary to introduce a baseline with a sudden appearance at a time Δt_{BL}, and an exponential decay (τ_{BL}) to another, constant baseline. This baseline, which applies over a wide range of energies, not just the Rydberg resonances, is interpreted as representing the signal of the hot, structurally disperse HT. This aspect is further discussed below, where we also discuss other spectral signatures that yield the onset of HT creation. The total experimentally observed intensity for each Rydberg state is then described by $I_{\mathrm{Ry}}(t)$ plus the baseline, convoluted with a Gaussian instrument function σ_{IF}:

$$I(t) = \int_0^t \mathrm{d}t' \left[a_1 I_{\mathrm{Ry}}(t) + a_2\, \mathrm{e}^{t-\Delta t_{\mathrm{BL}}/\tau_{\mathrm{BL}}} + a_3 H[(t-t') - \Delta t_{\mathrm{BL}}]\right] \mathrm{e}^{-(t-t')^2/2\sigma_{\mathrm{IF}}{}^2} \tag{2}$$

with adjustable parameters a_1, a_2, and a_3 to reflect the different intensities of the various signals, and where $H[(t-t') - \Delta t_{\mathrm{BL}}]$ is the Heaviside step function. The fits, Figure 5, adequately describe the experimental data. The fit parameters are summarized in Table 1.

Table 1. Experimentally Determined Dynamic Parameters for the Rydberg Peaks

Rydberg state	binding energy [eV]	τ_{1B} [fs]	$\Delta\tau$ [fs]	σ [fs]
6s	0.57	35	2	3
5p	0.78	33	3	2
4p	1.03	32	10	8
4s	1.27	33	11	1
3d′	1.45	33	17	9
3d	1.67	33	21	6
3p	2.26	36	27	24

Each of the Rydberg peak fits gives an experimental value for the lifetime of the 1B state, τ_{1B}. The average over these values, 34 fs, is in good agreement with the 30 fs lifetime obtained from fits of the direct spectral signature of 1B measured in the ionization experiments with shorter probe wavelengths as described earlier. The travel times Δt of the wavepacket, i.e., the time elapsed from entering the 2A state to reaching the resonance windows of the Rydberg states 6s through 3p ranges from 2 to 27 fs, with the peaks at higher binding energies appearing later. The fits also give values for the appearance of the baseline (178 fs) and the initial decay of this signal (72 fs). However, since the intensity of the baseline in all of the signals is below 3%, we consider those values to be less reliable than the ones discussed later.

The widths in time, σ, of the ionization windows for the Rydberg states 6s through 3d are very short, on the order of a few femtoseconds (Table 1). Only the ionization window for the 3p state is open somewhat longer, 24 fs. The variations between the resonance window widths outside of 3p are not statistically significant. To explain the short opening of the resonance windows, we note that to induce the transition from the 2A state to a Rydberg level the photon energy must match the difference between the electronic states and the momentum of the traveling wavepacket must be conserved. Because of the different electronic structures of the Rydberg states and the 2A state, it is likely that this resonance condition is, for each laser wavelength, met for only very specific locations on the reacting surface, explaining the short duration of the resonance windows.

The short persistence time of the resonance windows is consistent with the finding that the binding energies of the observed Rydberg peaks do not change with time. Because the binding energy of a Rydberg state depends on the structure of its ion core,[59] if the windows were open for extended periods one would expect the time dependence of the molecular structure to result in time-dependent binding energies, but such a time-dependence is not observed. We note also that since the Rydberg states are seen at different times Δt in the reaction process, their binding energies represent different molecular structures, each captured at a particular moment in time. Indeed, we show below that the binding energy of the transient 3p Rydberg peak differs from that of the CHD molecule when excited from its ground state structure.

At the time point where a Rydberg level is in the resonance window, the energy provided by the photon (assuming a one-photon excitation to the Rydberg level) must match the differences in the potential energies between the Rydberg state and the 2A state. Consequently,

$$h\nu = E^{\mathrm{D_0}}(\Delta t) - E_{\mathrm{B}}^{\mathrm{Ryd}}(\Delta t) - E^{\mathrm{2A}}(\Delta t)$$

or

$$E_{\mathrm{B}}^{\mathrm{Ryd}}(\Delta t) + h\nu = E^{\mathrm{D_0}}(\Delta t) - E^{\mathrm{2A}}(\Delta t) \tag{3}$$

where we denote by $E^{\mathrm{2A}}(\Delta t)$ the potential energy of the molecule in the 2A state at travel time Δt, and $E^{\mathrm{D_0}}(\Delta t)$ the potential energy of the D_0 ground state of the molecular cation of the ion at that time.

The binding energy of the Rydberg state observed at a time delay Δt is $E_{\mathrm{B}}^{\mathrm{Ryd}}(\Delta t)$. The measured binding energy is independent of the vibrational excitation of the molecule,[40,59,60] as is the difference between the ion and the molecule in 2A, assuming preservation of the kinetic nuclear energy in a sudden

DOI: 10.1021/acs.jpca.5b05672
J. Phys. Chem. A 2015, 119, 8832–8845

ionization process. Vibrational energy does therefore not enter eq 3.

Equation 3 establishes a relationship between the time-dependent observation of the binding energy, $E_B^{Ryd}(\Delta t)$, and the difference between the potential energies of the ion and the 2A state at the time of observation. The latter, but as a function of molecular coordinates, is usually computed in calculations of the molecular reaction path. A combination of the experimental, time-dependent results with the computational, position-dependent results should therefore yield a relationship between the reaction time and the position on the potential energy surface, i.e., the motion of the system down the reaction path.

To evaluate the molecular reaction dynamics in this way, the potential energy surfaces of CHD have been calculated along the symmetric reaction path. The calculations were done using the computational method described in the experimental section. Figure 6 shows the potential energy surfaces as a function of the distance between the carbon atoms C_1 and C_6, the termini in the HT molecule, along the ring-opening reaction coordinate.

It appears from Figure 6, where the pump is represented by a light blue arrow drawn to scale to reflect an energy of 4.69 eV, that the initial excitation takes the molecule directly into the 2A state. Clearly, this is not what happens. Previous experiments located the (vertical) transitions to 1B and 2A at 4.94 and 5.39 eV, respectively.[47] The MSCASPT2 calculation gives (adiabatic) excitation energies of 4.41 and 4.85 eV for the 1B and 2A states, respectively, which seems to be in reasonable agreement when accounting for the difference between vertical and adiabatic excitation.

We point out that the ionization energies were calculated for a C_2 symmetric reaction path. However, as has been postulated previously,[7−9] the reaction mechanism features symmetry breaking motions in 2A. Consequently, the energy along the reaction path is likely somewhat lower than represented by the 2A curve in Figure 6. Nonetheless, the figure shows that the energy required to excite the (6s−3p) Rydberg states out of 2A matches the probe photon energy at different locations along the reaction path between the 1B/2A CI and the decay back to the ground state. This is in agreement with the time-resolved spectra that follow the reaction without a gap, supporting the fact that we do indeed see the bottom of the 2A well.

We now connect the experimental results to the computational results with the aim to derive the time-dependent reaction dynamics of the molecule. Figure 7A graphs, for the Rydberg levels observed with 3.07 eV ionization pulses, the travel time as a function of the Rydberg levels' binding energy plus the photon energy (data from Table 1). Surprisingly, the binding energies of the accessed Rydberg states are seen to trend linearly with the travel time (slope: 16.6 fs/eV). There seems to be little to suggest a linear relationship so that the apparent linearity must be considered an accidental one. From the computed potential energy surfaces, Figure 6, we extract the separation of the terminal carbon atoms as a function of the difference between the ion energy and the energy of the 2A state, Figure 7B. Since the quantities plotted as a function of time (Figure 7A) and as a function of C_1−C_6 distance (Figure 7B) should be equal as per eq 3, we can relate the distance between the carbon atoms to the travel times (dashed lines). From that we obtain Figure 7C, which shows the terminal

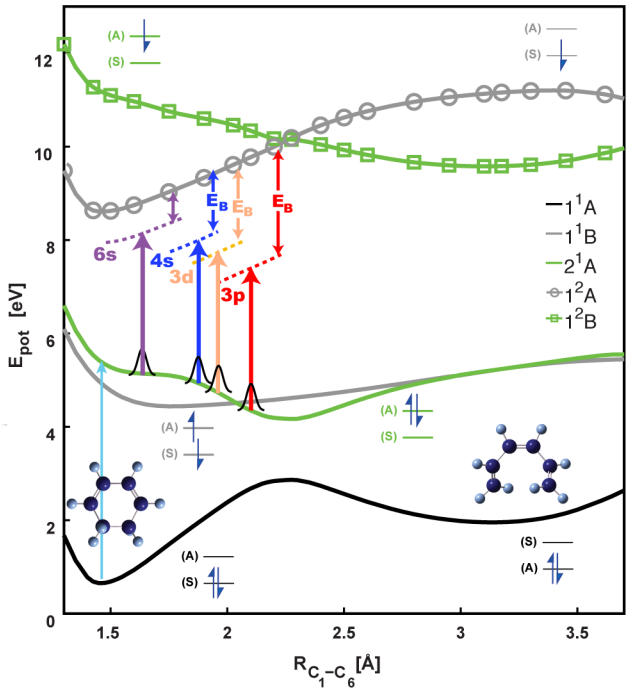

Figure 6. Potential energy surfaces of the CHD−HT system, computed at the MS-CASPT2 level along the C_2 symmetric minimum energy reaction path. The electronic ground state, black, connects CHD to HT via an energy barrier. The gray curves represent the 1B electronic state (no symbols) and the 1A ion state (circles) that are reached by removing one electron from the 1B excited state configuration. The green curves represent the 2A electronic state (no symbols) and the 1B ion state (squares) reached by removing one electron from the 2A excited state configuration. The dominant electron configurations in each state are indicated. The symmetric orbital (S) is the HOMO in ground state CHD and the LUMO in HT. The antisymmetric orbital (A) is the HOMO in ground state HT and the LUMO in ground state CHD. The vertical arrows indicting the probe photons are drawn to scale. They lead to Rydberg states, dashed lines, which are drawn at the molecular geometry corresponding to the transition. The potential energies with respect to the ion energy, i.e., the BE (represented by the double-sided arrows), are experimentally measured and also drawn to scale. The resonance windows for the transitions are illustrated by Gaussians. The up-arrows portraying the probe photons at different stages of the reaction are drawn at the C_1−C_6 distances determined here.

carbon distance $R_{C_1-C_6}$ as a function of reaction time on the 2A surface, Δt.

We note that the 6s resonance window occurs very early in the reaction on 2A and with a small change of the molecular structure. This is a rational result in light of our discussion of the lack of structural evolution in the 1B state: since 1B dephases into 2A before it can travel down the reaction path, the structure of the molecule does not evolve much in the 1B lifetime. Once in 2A, the 6s resonance window is reached after 2 fs, which is too short a time to significantly change the structure.

From this analysis it follows that as the molecule reacts on the 2A surface, the distance between the terminal carbon atoms increases, apparently again almost linearly, from an initial value of about 1.65 Å, near to the equilibrium bond length in CHD, to a value of 2.1 Å that is near the crossing point to the ground state. During this motion on the 2A surface, the terminal carbon distance increases with a speed of 16 Å/ps.

DOI: 10.1021/acs.jpca.5b05672
J. Phys. Chem. A 2015, 119, 8832−8845

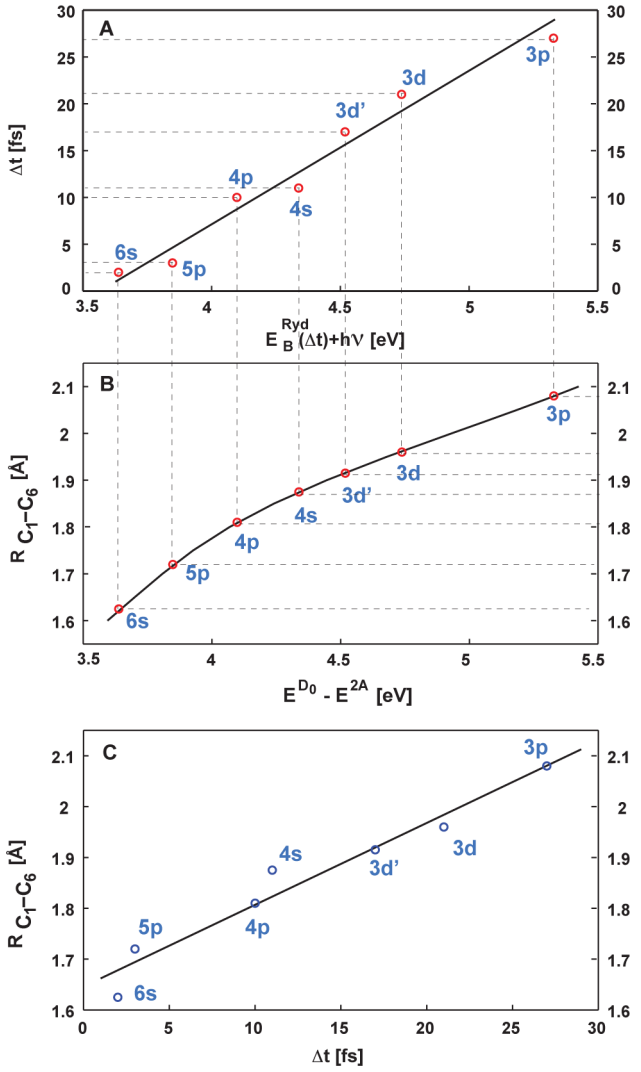

Figure 7. (A) Experimentally measured travel times of the wavepacket on the 2A surface to the resonance window for photoionization via the observed Rydberg states as a function of the combined binding and photon energy (eq 3). (B) Calculated distance between the terminal carbon atoms, $R_{C_1-C_6}$, as a function of the energy difference between the 2A state and the ground state ion. The dashed lines in panels A and B connect the distance between the terminal carbon atoms and the travel time since the energy scales are equal (eq 3). (C) Derived structural parameter $R_{C_1-C_6}$ as a function of wavepacket travel time.

With the time-dependent structure at hand, we can evaluate the energetics of the molecule during the reaction on the 2A state. Using the method presented in Figure 7, panels A and B, we determine the structural parameter $R_{C_1-C_6}$ associated with each Rydberg state. From the data presented in Figure 6, it is possible to obtain the computed 2A potential energy corresponding to each respective resonance window. Given that, and given the total energy deposited by the pump laser photon, we can now obtain the time dependence of the kinetic energy, Figure 8. A linear fit of the data presented in Figure 8 shows that as the wavepacket moves down the potential energy surfaces it acquires kinetic energy at a rate of 28 eV/ps.

In the analysis presented here, we have determined the time-dependent molecular structure by clocking the travel times to the resonance windows. These resonance windows are at well-defined locations where the energy between the Rydberg state

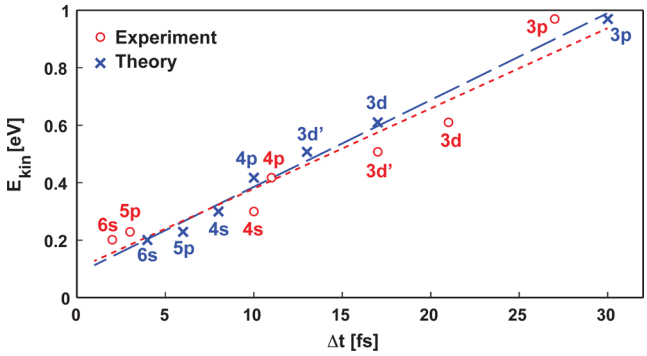

Figure 8. Kinetic energy of the wavepacket as a function of travel time in 2A as determined by the experiment (red circles and dotted line) and the computation (blue symbols and dashed line). Kinetic energies at the locations of the Rydberg state resonance windows, for both the experimental and calculated travel times, were obtained by subtracting the potential energy of 2A at the corresponding $R_{C_1-C_6}$ (Figure 6), from the total energy deposited by the pump photon.

and the 2A state matches the photon energy. We have calculated these locations at the MS-CASPT2 level. While this calculation gives good agreement with experimental excitation and ionization energies, the applicability of this calculation to the analysis must be examined. The calculation shows a point of degeneracy (the CI) between 1B and 2A at a C_1-C_6 distance of 2.05 Å. If we assumed that the geometry of this degeneracy was exactly where the transition to 2A takes place then the gaps between 2A and the (6s−4s) Rydberg states would match our photon energies at locations along the reaction path, where the wavepacket would still be in 1B. While it is well established that the wavepacket circumvents the C_2 symmetric CI in a symmetry breaking motion,[7,9,15] Figure 6 displays the C_2 symmetric minimum energy structures. We view the calculated ionization energies along that minimum energy path as reasonable approximations of the energies required to reach the Rydberg states out of various locations along the 2A state. Consequently, the structural dynamics parameters obtained in Figures 7 and 8 should be viewed as approximate.

At this juncture, it is interesting to compare the currently measured travel times with the travel times implied by recent time-resolved structural dynamics experiments using pulsed X-rays at the LCLS.[33] There, the analysis of the experiment resulted in a set of eight weighted trajectories for the CHD ring-opening reaction, each trajectory representing a separate component of the nonadiabatic nuclear-electronic wavepacket. Here, we use the same eight trajectories to calculate the resonant photoionization via Rydberg states, using the following approximation:

$$\sigma_{\mathrm{ion}}^{\mathrm{Ryd}}(t') = \sum_{k=1}^{N=8} w_k \int_{-\infty}^{\infty} \sum_i |a_k^{(i)}(t)|^2 \, d_{\mathrm{res}}(\Delta E_k^{(i,\mathrm{Ryd})}(t)) \varepsilon_{\mathrm{probe}}(t - t') \, \mathrm{d}t \tag{4}$$

where w_k are the weights of the trajectories, coefficients $a_k^{(i)}(t)$ the amplitudes on each of the electronic states, and $d_{\mathrm{res}}(\Delta E_k^{(i,\mathrm{Ryd})}(t))$ the resonance windows for the valence-to-Rydberg transition given by a normalized Lorentzian function with a 0.15 eV width, and resonance energy $\Delta E_k^{(i,\mathrm{Ryd})}(t) = E_k^{(i)}(t) + E_B^{\mathrm{Ry}} + h\nu - E_k^{D_0}(t)$, where $E_k^{(i)}$ is the energy of electronic state i, E_B^{Ry} the experimentally determined Rydberg binding energy, $E_k^{D_0}$ the energy of the D_0 ground state of the molecular cation, and finally, $h\nu$ the photon energy. The molecular

DOI: 10.1021/acs.jpca.5b05672
J. Phys. Chem. A 2015, 119, 8832−8845

energies are calculated at the MS-CASPT2/cc-pVDZ level of *ab initio* theory. The signal is convoluted by the probe pulse, which is represented by a normalized Gaussian, with t' the delay time between pump and probe. This analysis, which combines the results from the ultrafast X-ray scattering experiments with an approximate calculation of the resonant ionization signal, results in travel times that are Δt = 4 (6s), 6 (5p), 8 (4p), 10 (4s), 13 (3d′), 17 (3d), and 30 (3p) in fs. These times agree approximately with the current spectroscopic analysis presented in the fourth column of Table 1. It indicates a qualitative agreement between the two completely different experiments, ultrafast structural dynamics on one hand and ultrafast spectroscopy on the other. It is worth noting that the symmetric C_2 stretch is not the dominant reaction coordinate for the trajectories and that most trajectories reach the diabatic S_1/S_2 crossing rather soon, which leads to the S_1 curve changing diabatic character from 1B (in the Franck−Condon region) to 2A. This can be thought of as a 1B−2A transition induced by dynamics.

Finally, a separate approach to determine the time-dependent molecular structures would be to calculate the Rydberg electron binding energies, which depend on the molecular structure. For any proposed molecular structure along the ring-opening pathway, one could calculate the binding energies of the Rydberg levels and compare to experimental values. By varying the laser wavelength of the probe pulse, the time-evolution of the binding energies throughout the reaction path could be measured and, by comparison to the calculation, the complete time-dependent molecular structure could be determined. The present experiments did not pursue this approach because only for one wavelength did we have sufficient intensity to observe the Rydberg levels and because the Rydberg state binding energies of the molecule along the reaction path are difficult to calculate.

Arriving at the Hexatriene Product. The direct observation of the 1B state and the temporally sequenced Rydberg peaks reveal the movement of the wavepacket on the 2A surface. To complete the view of the ring-opening dynamics through all its stages, we explore next the formation of the nascent reaction product, HT.

Figure 9 displays the 4.69 eV pump/3.07 eV probe time-resolved photoelectron spectrum out to 5 ps pump−probe time delay. At delay times beyond ∼200 fs a broad, unresolved feature appears that has been assigned previously to the open-chain structure of HT.[61] If CHD were to return to its original ground state structure, the photoionization by the probe photon would give a binding energy spectrum just like the original molecule, even though it has 4.69 eV in excess vibrational energy.[61] In that case Figure 9 would show no signal after the passage through the 2A state. The fact that there is a signal, albeit broad, implies that a new molecular structure, the HT structure, is created in the reaction. In total, HT can have six different structures: three conformeric forms of where the central double bond has cis geometry and three conformeric forms from where it is trans.[62] The initial photoproduct has a gZg-geometry, even though the partially folded structures labeled tZc and tZt are the most stable ones.[63,64] The barriers between these structures are below the energy present in the molecule following the ring-opening reaction so that the reaction leads to a product that can assume a multitude of conformeric forms. Rudakov et al. have argued that this structural dispersion causes the broadness of the difference signal observed for the vibrationally hot product in Figure 9.[61]

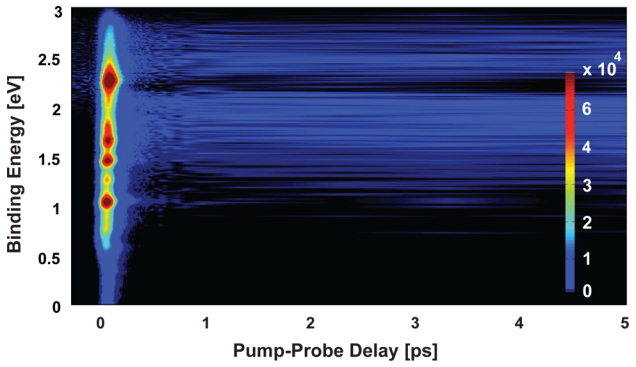

Figure 9. Time-dependent Rydberg electron binding energy spectrum of CHD upon excitation with 4.69 eV (265 nm) pump photons on a picosecond time scale. The reaction progress is probed by multiphoton ionization photoelectron spectroscopy using 3.07 eV (404 nm) pulses. All one-color signals have been subtracted. The color scale was adjusted to enhance the contrast of the low intensity region.

The dip in spectral intensity near 2.2 eV results from the depletion of ground state CHD after absorption of the pump photon. The direct transition from CHD in its electronic ground state to the 3p state is located near 6 eV so that two probe photons can lift the molecule into 3p. In the one-color spectra taken with probe pulses only, a single peak corresponding to 3p therefore dominates the binding energy spectrum. In the two-color spectra where the probe pulse comes before the pump pulse, this peak also dominates the spectrum. In the two-color spectrum with the pump pulse before the probe pulse, there is a little less ground state CHD because absorption of a pump photon and subsequent loss of the closed ring structure reduces the number of ground state CHD molecules in the molecular beam. Consequently, there is a reduced contribution of the one-color probe background to the total signal. This reduction of one-color background signal leads to an oversubtraction of background in the spectrum at positive times.

To extract the spectrum of the pure, nascent HT produced in the reaction, we subtract the spectrum with negative time delay from the spectrum with positive time delay following the procedure of Rudakov et al.[61] From this we find that 4% of the CHD is excited to the reacting 1B state. As intended, this fraction of excitation is small, giving confidence that our experiment explores the dynamics of single-photon excited molecules.

The HT spectrum derived here and previously reported by Rudakov et al., inset in Figure 10, shows a single broad peak stretching from less than 1.5 eV to about 2.8 eV of binding energy. Similar to CHD, HT has an ionization energy of about 8.30 eV, slightly dependent on the conformeric structure.[52,65−67] Like in CHD, two probe pulse photons can excite to the 3p level, from where a single photon can ionize the molecule. Even while the broadness of the peak could be ascribed to the structural dispersion in the nascent HT, the fact that it reaches as low as 1.5 eV is interesting. It is conceivable that a breakdown of the Δv = 0 selection rule for ionizing the molecule out of the 3p Rydberg state contributes to the broadening. Strictly speaking this selection rule applies to molecules in harmonic potentials.[40] It breaks down when molecules are structurally disperse and when the potentials are not harmonic. In the present case of HT created with large amounts of internal energy, the energy is sufficient for the

DOI: 10.1021/acs.jpca.5b05672
J. Phys. Chem. A 2015, 119, 8832−8845

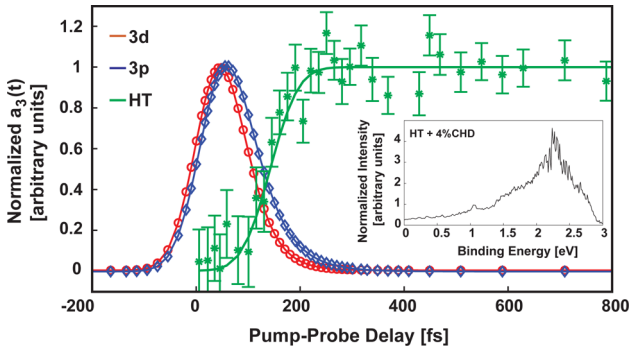

Figure 10. Time dependence of the 3d and 3p Rydberg states and HT in the pump−probe experiment with 265 and 404 nm. The error bars depict the 95% confidence interval of the nonlinear regression parameters. The lines represent the dynamic fits for the time dependence of the 3d, 3p, and HT signals. Inset: The spectrum of the nascent HT reaction product, obtained according to the procedure of ref 61.

molecule to distribute over multiple structures. The harmonic approximation may therefore break down, enabling $\Delta v \neq 0$ ionization transitions that remove or insert energy from or into vibrations, respectively. In the binding energy spectrum, this would be manifest as a peak broadening.

In order to follow the appearance of HT relative to the evolution of the Rydberg progression, the broad HT spectrum has to be deconvoluted from the overall spectrum at pump−probe delays where both, the Rydberg progression and the HT product, are present. As noted, this was accomplished by deconvoluting the HT spectrum from the Rydberg progression in the binding energy region between 1.6 and 3.1 eV, where the HT spectrum has maximum intensity. To fit the time-dependent spectrum in this energy range, the spectrum at each time point was fitted to a weighted sum of four Gaussian peaks (one for each of the 3d Rydberg peaks; two Gaussians were needed to fit the 3p peak) plus the experimental HT spectrum. The resulting time-dependencies of the 3d, 3p, and HT signals are shown in Figure 10. The 3d and 3p signals and fits are the same as the ones drawn in Figures 2 and 5, but shown here again to illustrate the delayed rise of the HT signal. The fits of 3d and 3p used mathematical expressions similar to eqs 1 and 2. Since the signal for the hot, structurally disperse structure is eliminated in the deconvolution, the stepfunction was removed from these fits.[48] Instead, the HT signal was fit separately to a step function centered at Δt_{BL}.

The analysis reveals HT to appear at a time of 142 fs after the optical excitation and to closely follow the decay of the 3p state. This suggests that the resonance window associated with the 3p Rydberg peak is at or near the bottom of the 2A surface, which is consistent with the discussion of the previous section. It also explains why the 3p resonance window is open for a measurable time (Table 1). The value of 142 fs is in very good agreement with previously reported times for the lifetime of 2A, which was given as 130−139 fs.[7,27,28] Our experiment does not show any decay or change of the shape of the HT spectrum up to a maximum time delay of 14 ps. This suggests that, within this time frame, there is no further vibrational or rotational relaxation of the HT molecule. UV transient absorption measurements in various solvents determined the vibrational cooling and thermal equilibration of HT with its surroundings to proceed on a time scale of 10−30 ps, depending on the solvent.[61,68−70] In the low density environment of the molecular beam, where no collisions can facilitate such relaxation, vibrational cooling time scales must be much larger.

In total, the time-resolved photoelectron spectrum of the ring-opening reaction covers the entire time range from the initiation of the reaction in the 1B state to the creation of the nascent hexatriene molecule. We observe the initially photo-excited 1B valence state, the sequence of Rydberg peaks that reveal the dynamical motion of the wavepacket as it descends the steep reaction path, up to and including the formation of hexatriene with a fully disperse molecular structure.

SUMMARY AND PERSPECTIVES

For the electrocyclic ring-opening reaction of 1,3-cyclohexadiene to 1,3,5-hexatriene, all steps predicted in the van der Lugt Oosterhof model,[10] from the initially excited state to the product, have been observed via photoelectron spectroscopy. While building on a significant number of prior studies, our results clarify, revise, and promote our knowledge about the ring-opening of CHD in several ways. The direct observation of 1B, supported by the analysis of the dynamical signatures of the Rydberg levels, provides a new lifetime of 30 fs for the optically excited state. This is shorter than the previously reported 53−56 fs lifetime derived from high intensity mass spectrometry[7,27] and photoelectron spectroscopy.[28] The discrepancy with these prior measurements might be due to differences in the coherence bandwidth of the optical pulses that prepare the molecules in the excited state.

On the 2A surface, we now are able to uncover the sequential appearance of the Rydberg peaks, which allows us to determine their origin. A dynamical fit shows that excitation out of 2A happens while the wavepacket transits very narrow windows where resonance excitation to a Rydberg state is possible. Since these windows must be positions where the energy difference between the 2A and the respective Rydberg state matches the laser photon energy, we are able to establish the delay times at which these potential energy curves have the required energy difference. Coupling to computational results obtained at the MS-CASPT2 level allows us to relate our measurements to time-varying molecular structures. As the molecule slides down the 2A surface, it converts potential energy into kinetic energy at a rate of 28 eV/ps, while the terminal carbon atoms separate with a speed of 16 Å/ps. The experiment shows these rates to be nearly linear. Of course, energy is distributed in a multitude of coordinates, so that there is no inherent contradiction in the apparent linearity of both processes.

Although the travel times to the resonance windows obtained from the dynamic fits of the Rydberg signals agree quite well with the theoretical analysis based on quantum molecular dynamics trajectories, some important questions remain. In particular, the initial decay time $\tau_{1B} \approx 30$ fs observed in the experiment is a source of discrepancy between experiment and theory. This exponential decay, which has been observed with slightly larger time constants in prior experiments, does not have an obvious counterpart in the calculated trajectories where the nuclear dynamics on the 1B/2A diabatic states is triggered immediately by the optical pump pulse. There are several possible explanations, ranging from an inaccurate topology of the potential energy surface in the Franck−Condon region to not accounting for the structural dependence of photo-ionization cross sections. On the experimental side, there is a possibility that the optical pump pulse is chirped or simply that the pump and probe pulses are not sufficiently short. Finally, it is possible that spreading of the traveling wavepacket mimics

DOI: 10.1021/acs.jpca.5b05672
J. Phys. Chem. A 2015, 119, 8832−8845

the mathematical form of an exponential decay. Future explorations with higher time resolution might yield further insights.

The time-resolved signature of the optically excited 1B state reveals no significant structural evolution, at least on the time scale of its lifetime that is limited by rapid decay into the 2A state. It should be noted that this does not affect the prior interpretation of the origin of the Woodward−Hoffmann conrotatory pathway of the reaction as resulting from an out-of-plane twisting of the carbon atoms corresponding to the termini in the open chain isomer. This motion aligns the orbital lobes of these atoms favorably for a double bond forming interaction with the neighboring carbons. While this vibration is still instrumental for defining the Woodward−Hoffmann reaction path, its motions are about an equilibrium position that does not evolve on the time scale of its decay. In contrast, the minimum energy path calculations of Garavelli et al.[7] had suggested that a large out-of-plane motion of the termini leads to a new minimum energy structure and the steeply sloped potential of 1B.

The total reaction time, from absorption of a photon to product formation, was found to be 142 fs, which is in remarkable agreement with prior investigations.[7,27,28] The results are also consistent with the outcome of recent time-resolved X-ray diffraction experiments that we conducted using the ultrafast LCLS X-ray source. In those experiments we observed the time evolving molecular structure as the reaction proceeds. These data served as the arbiter to determine which, of a multitude of computated trajectories, are the ones that dominate the reaction. The movie of the reaction, which is provided with the diffraction study,[33] is in agreement with the photoelectron results presented here. In particular we point out that the movie shows the molecule performing about 1.5 oscillations in a high frequency carbon skeleton oscillation before the bond breaks to form hexatriene. Given the 22 fs time scale of the vibrational motions in 1B, the experimentally determined lifetime of 30 fs for the 1B state is consistent with the computational simulations, and by implication the diffraction results. The travel times on the 2A surface determined from the time-resolved spectroscopy are also in substantial agreement with those from the simulation of the X-ray diffraction results.

Our dynamic analysis mapped the Rydberg electron binding energy as the reaction unfolds. In the present study we have resorted to calculations of the 2A surface and the ion surface to derive the structural dynamics. However, the experimental observation of the time-dependent Rydberg state binding energies lends itself to extract the time-dependent structure in a different way. Once it is possible to calculate the Rydberg electron binding energy as a function of molecular structure, one could derive the molecular structure independently of the diffraction results. This is so because the binding energy of Rydberg electrons has been closely associated with the molecular structure. Indeed, we note that the binding energy of the transient 3p Rydberg state accessed from the 2A surface (2.26 eV) differs from that of CHD in its ground state structure, obtained in the same experiment via 1-C 3-photon ionization (2.23 eV[48]): there is clearly structural information in our spectra that we are not yet able to decipher. Consequently, with further advances in computational technology, we might be able to watch the reaction of CHD from two very different viewpoints, namely, a spectroscopic view and a diffraction view, which could further solidify our understanding of this reaction. We note that impressive advances have recently been made in the computation of Rydberg electron binding energies.[35,36]

The possibility has been raised that the ionization experiments may have looked at a minor fraction of the excited molecules, while most of them react in a different, unobserved way.[18] The present study with improved signal and complete time coverage finds no indication of hidden reaction pathways that remain undetected. It consequently seems unlikely that hidden paths with significant populations exist.

AUTHOR INFORMATION

Notes

The authors declare no competing financial interest.

ACKNOWLEDGMENTS

This project benefited from support by the National Science Foundation, grant number CBET-1336105, and by the Defense Threat Reduction Agency (DTRA), Grant No. HDTRA1-14-1-0008. A.K. and K.S. acknowledge grants FP7-PEOPLE-2013-CIG-NEWLIGHT (European Union) and RPG-2013-365 (The Leverhulme Trust).

REFERENCES

(1) Klessinger, M.; Michl, J. *Excited States and Photochemistry of Organic Molecules*; VCH: New York, 1995.
(2) Feldman, D.; Glorieux, F. H.; Pike, J. W. *Vitamin D*; Academic: San Diego, CA, 1997.
(3) Wolak, M. A.; Gillespie, N. B.; Thomas, C. J.; Birge, R. R.; Lees, W. Optical Properties of Photochromic Fluorinated Indolylfulgides. *J. Photochem. Photobiol., A* **2001**, *144*, 83−92.
(4) Turro, N. J.; Scaiano, J. C. Ramamurthy. V.; *Modern Molecular Photochemistry of Organic Molecules*; USB: Sausalito, CA, 2010.
(5) Woodward, R. B.; Hoffmann, R. The Conservation of Orbital Symmetry. *Angew. Chem., Int. Ed. Engl.* **1969**, *8*, 781−853.
(6) Longuet-Higgins, H. C.; Abrahamson, E. W. The Electronic Mechanism of Electrocyclic Reactions. *J. Am. Chem. Soc.* **1965**, *87*, 2045−2046.
(7) Garavelli, M.; Page, C. S.; Celani, P.; Olivucci, M.; Schmid, W. E.; Trushin, S. A.; Fuss, W. Reaction Path of a Sub-200 fs Photochemical Electrocyclic Reaction. *J. Phys. Chem. A* **2001**, *105*, 4458−4469.
(8) Schönborn, J. B.; Sielk, J.; Hartke, B. Photochemical Ring-Opening of Cyclohexadiene: Quantum Wavepacket Dynamics on a Global Ab Initio Potential Energy Surface. *J. Phys. Chem. A* **2010**, *114*, 4036−4044.
(9) Nenov, A.; Kölle, P.; Robb, M. A.; de Vivie-Riedle, R. Beyond the van der Lugt/Oosterhoff Model: When the Conical Intersection Seam and the S1 minimum Energy Path Do Not Cross. *J. Org. Chem.* **2010**, *75*, 123−129.
(10) van der Lugt, W. T. A. M.; Oosterhoff, L. J. Symmetry Control and Photoinduced Reactions. *J. Am. Chem. Soc.* **1969**, *91*, 6042−6049.
(11) Celani, P.; Ottani, S.; Olivucci, M.; Bernardi, F.; Robb, M. A. What Happens During the Picosecond Lifetime of 2A1 Cyclohexa-1,3-diene? A CAS-SCF Study of the Cyclohexadiene/Hexatriene Photochemical Interconversion. *J. Am. Chem. Soc.* **1994**, *116*, 10141−10151.
(12) Celani, P.; Bernardi, F.; Robb, M. A.; Olivucci, M. J. Do Photochemical Ring-Openings Occur in the Spectroscopic State? $^1B_2$ Pathways for the Cyclohexadiene/Hexatriene Photochemical Interconversion. *J. Phys. Chem.* **1996**, *100*, 19364−19366.
(13) Bernardi, F.; Olivucci, M.; Robb, M. A. Potential Energy Surface Crossings in Organic Photochemistry. *Chem. Soc. Rev.* **1996**, *25*, 321−328.
(14) Garavelli, M.; Celani, P.; Fato, M.; Bearpark, M. J.; Smith, B. R.; Olivucci, M. J.; Robb, M. A. Relaxation Paths from a Conical Intersection: The Mechanism of Product Formation in the Cyclohexadiene/Hexatriene Photochemical Interconversion. *J. Phys. Chem. A* **1997**, *101*, 2023−2032.

DOI: 10.1021/acs.jpca.5b05672
J. Phys. Chem. A 2015, 119, 8832−8845

(15) Tamura, H.; Nanbu, S.; Ishada, T.; Nakamura, H. *Ab initio* Nonadiabatic Quantum Dynamics of Cyclohexadiene/Hexatriene Ultrafast Photoisomerization. *J. Chem. Phys.* **2006**, *124*, 084313.
(16) Tamura, H.; Nanbu, S.; Nakamura, H.; Ishada, T. A Theoretical Study of Cyclohexadiene/Hexatriene Photochemical Interconversion: Multireference Configuration Interaction Potential Energy Surfaces and Transition Probabilities for the Radiationless Decays. *Chem. Phys. Lett.* **2005**, *401*, 487−491.
(17) Li, A.; Yuan, S.; Dou, Y.; Wang, Y.; Wen, Z. Semiclassical Dynamic Simulation of Photon Induced Ring-Opening. *Chem. Phys. Lett.* **2009**, *478*, 28−32.
(18) Deb, S.; Weber, P. M. The Ultrafast Pathway of Photon-Induced Electrocyclic Ring Opening Reactions: The Case of 1,3-Cyclohexadiene. *Annu. Rev. Phys. Chem.* **2011**, *62*, 19−39.
(19) Pullen, S. H.; Anderson, N. A.; Walker, L. A., II; Sension, R. J. The Ultrafast Photochemical Ring-Opening Reaction of 1,3-Cyclohexadiene in Cyclohexane. *J. Chem. Phys.* **1998**, *108*, 556−563.
(20) Pullen, S.; Walker, L. A.; Donovan, B.; Sension, R. J. Femtosecond Tansient Absorption Study of the Ring Opening Reaction of 1,3-Cyclohexadiene. *Chem. Phys. Lett.* **1995**, *242*, 415−20.
(21) Lochbrunner, S.; Fuss, W.; Schmid, W. E.; Kompa, K. L. Electronic Relaxation and Ground-State Dynamics of 1,3-Cyclohexadiene and *cis*-Hexatriene in Ethanol. *J. Phys. Chem. A* **1998**, *102*, 9334−9344.
(22) Trulson, M. O.; Dollinger, G. D.; Mathies, R. A. Femtosecond Photochemical Ring Opening Dynamics of 1,3-Cyclohexadiene from Resonance Raman Intensities. *J. Am. Chem. Soc.* **1987**, *109*, 586−587.
(23) Trulson, M. O.; Dollinger, G. D.; Mathies, R. A. Excited State Structure and Femtosecond Ring-Opening Dynamics of 1,3-Cyclohexadiene from Absolute Resonance Raman Intensities. *J. Chem. Phys.* **1989**, *90*, 4274−4281.
(24) Lawless, M. K.; Wickham, S. D.; Mathies, R. A. Resonance Raman view of Pericyclic Photochemical Ring-Opening Reactions: Beyond the Woodward-Hoffmann Rules. *Acc. Chem. Res.* **1995**, *28*, 493−502.
(25) Dudek, R. C.; Weber, P. M. Ultrafast Diffraction Imaging of the Electrocyclic Ring-Opening Reaction of 1,3-Cyclohexadiene. *J. Phys. Chem. A* **2001**, *105*, 4167−4171.
(26) Bühler, C. C.; Minitti, M. P.; Deb, S.; Bao, J.; Weber, P. M. Ultrafast Dynamics of 1,3-Cyclohexadiene in Highly Excited States. *J. At., Mol., Opt. Phys.* **2011**, *2011*, 1.
(27) Kosma, K.; Trushin, S. A.; Fuß, W.; Schmid, W. E. Cyclohexadiene Ring Opening Observed with 13 fs Resolution: Coherent Oscillations Confirm the Reaction Path. *Phys. Chem. Chem. Phys.* **2009**, *11*, 172−181.
(28) Kuthirummal, N.; Rudakov, F.; Evans, C. L.; Weber, P. M. Spectroscopy and Femtosecond Dynamics of the Ring Opening Reaction of 1,3-Cyclohexadiene. *J. Chem. Phys.* **2006**, *125*, 133307.
(29) Schick, C. P.; Weber, P. M. Ultrafast Dynamics in Superexcited States of Phenol. *J. Phys. Chem. A* **2001**, *105*, 3725−3734.
(30) Schick, C. P.; Weber, P. M. Ultrafast Dynamics in the 3-Photon Double Resonance Ionization of Phenol via the S_2 Electronic State. *J. Phys. Chem. A* **2001**, *105*, 3735−3740.
(31) Piecuch, P.; Hansen, J. A.; Staedter, D.; Faure, S.; Blanchet, V. Communication: Existence of the Doubly Excited State that Mediates the Photoionization of Azulene. *J. Chem. Phys.* **2013**, *138*, 201102.
(32) Adachi, S.; Sato, M.; Suzuki, T. Direct Observation of Ground-State Product Formation in a 1,3-Cyclohexadiene Ring-Opening Reaction. *J. Phys. Chem. Lett.* **2015**, *6*, 343−346.
(33) Minitti, M. P.; Budarz, J. M.; Kirrander, A.; Robinson, J. S.; Ratner, D.; Lane, T. J.; Zhu, D.; Glownia, M.; Kozina, M. E.; Sikorski, M.; et al. Imaging Molecular Motions: Femtosecond X-Ray Scattering of an Electrocyclic Chemical Reaction. *Phys. Rev. Lett.* **2015**, *114*, 255501.
(34) Minitti, M. P.; Budarz, J. M.; Kirrander, A.; Robinson, J. S.; Lane, T. J.; Ratner, D.; Saita, K.; Northey, T.; Stanus, B.; Cofer-Shabica, V.; et al. Toward Structural Femtosecond Chemical Dynamics: Imaging Chemistry in Space and Time. *Faraday Discuss.* **2014**, *171*, 81−91.
(35) Gudmundsdóttir, H.; Zhang, Y.; Weber, P. M.; Jónsson, H. Self-Interaction Corrected Density Functional Calculations of Molecular Rydberg States. *J. Chem. Phys.* **2013**, *139*, 194102.
(36) Cheng, X.; Zhang, Y.; Deb, S.; Minitti, M. P.; Gao, Y.; Jónsson, H.; Weber, P. M. Ultrafast Structural Dynamics in Rydberg Excited *N*, *N*, *N*′, *N*′-Tetramethylethylenediamine: Conformation Dependent Electron Lone Pair Interaction and Charge Delocalization. *Chem. Sci.* **2014**, *5*, 4394−4403.
(37) Bao, J.; Weber, P. M. Ultrafast Dynamics of Highly Excited Trans-Stilbene: A Different Twist. *J. Phys. Chem. Lett.* **2010**, *1*, 224−227.
(38) Cardoza, J. D.; Rudakov, F. M.; Weber, P. M. Electronic Spectroscopy and Ultrafast Energy Relaxation Pathways in the Lowest Rydberg States of Trimethylamine. *J. Phys. Chem. A* **2008**, *112*, 10736−10743.
(39) Kim, B.; Thantu, N.; Weber, P. M. High Resolution Photoelectron Spectroscopy: The Vibrational Spectrum of the 2-Aminopyridine Cation. *J. Chem. Phys.* **1992**, *97*, 5384−5391.
(40) Minitti, M. P.; Cardoza, J. D.; Weber, P. M. Rydberg Fingerprint Spectroscopy of Hot Molecules: Structural Dispersion in Flexible Hydrocarbons. *J. Phys. Chem. A* **2006**, *110*, 10212−10218.
(41) Werner, H.-J.; Knowles, P. J. A Second Order Multiconfiguration SCF Procedure with Optimum Convergence. *J. Chem. Phys.* **1985**, *82*, 5053−5063.
(42) Knowles, P. J.; Werner, H.-J. An Efficient Second-Order MC SCF Method for Long Configuration Expansions. *Chem. Phys. Lett.* **1985**, *115*, 259−267.
(43) Dunning, T. H., Jr. Gaussian Basis Sets for Use in Correlated Molecular Calculations. I. The Atoms Boron Through Neon and Hydrogen. *J. Chem. Phys.* **1989**, *90*, 1007−1023.
(44) Werner, H.-J.; Knowles, P. J.; Knizia, G.; Manby, F. R.; Schütz, M.; et al. *MOLPRO*, version 2012.1, a package of ab initio programs; see http://www.molpro.net.
(45) Werner, H.-J. Third-Order Multireference Perturbation Theory: The CASPT3 Method. *Mol. Phys.* **1996**, *89*, 645−661.
(46) Finley, J.; Malmqvist, P.-Å.; Roos, B. O.; Serrano-Andrés, L. The Multi-State CASPT2 Method. *Chem. Phys. Lett.* **1998**, *288*, 299−306.
(47) Merchán, M.; Serrano-Andres, L.; Slater, L. S.; Roos, B. O.; McDiarmid, R.; Xing, X. Electronic Spectra of 1,4-Cyclohexadiene and 1,3-Cyclohexadiene: A Combined Experimental and Theoretical Investigation. *J. Phys. Chem. A* **1999**, *103*, 5468−76.
(48) Pemberton, C. C. The Reaction Path of Photoinduced Electrocyclic Ring-Opening: Ultrafast Spectroscopy of 1,3-Cyclohexadiene and α-Terpenine. Ph.D. Dissertation, Brown University, Providence, RI, 2015.
(49) McDiarmid, R.; Sabljc, A.; Doering, J. P. Valence Transitions in 1,3-Cyclopentadiene, 1,3-Cyclohexadiene and 1,3-Cycloheptadiene. *J. Chem. Phys.* **1985**, *83*, 2147−2152.
(50) A total of four Gaussians for each spectrum was necessary to obtain a good fit. The peaks around 2.2 and 1.6 eV were represented by one Gaussian each. Two additional Gaussians were needed to fit the background. On the higher binding energy side, a very noisy background is likely the result of imperfect subtraction of one color signal.
(51) Kimura, K.; Katsumata, S.; Achiba, Y.; Yamazaki, T.; Iwata, S. *Handbook of HeI Photoelectron Spectra of Fundamental Organic Compounds*; Japan Scientific Soc. Press: Tokyo, Japan, 1981.
(52) Bieri, G.; Burger, F.; Heilbronner, E.; Maier, J. P. Valence Ionization Energies of Hydrocarbons. *Helv. Chim. Acta* **1977**, *60*, 2213.
(53) Demeo, D. A.; El-Sayed, M. A. Ionization Potential and Structure of Olefins. *J. Chem. Phys.* **1970**, *52*, 2622.
(54) Heilbronner, E.; Hoshi, T.; von Rosenberg, J. L.; Hafner, K. Alkyl-induced, Natural Hypsochromic Shifts of the $^2A \leftarrow ^2X$ and $^2B \leftarrow ^2X$ Transitions of Azulene and Naphthalene Radical Cations. *Nouv. J. Chim.* **1976**, *1*, 105.
(55) Bischof, P.; Heilbronner, E. Photoelektron-Spektren von Cycloalkenen und Cycloalkadienen. *Helv. Chim. Acta* **1970**, *53*, 1677.
(56) Autrey, D.; Choo, J.; Laane, J. Spectroscopic Determination of the Ring-Twisting Potential Energy Function of 1,3-Cyclohexadiene

DOI: 10.1021/acs.jpca.5b05672
J. Phys. Chem. A 2015, 119, 8832−8845

and Comparison with Ab Initio Calculations. *J. Phys. Chem. A* **2001**, *105*, 10230−36.
(57) Weber, P. M.; Thantu, N. Photoionization via Transient States. A Coherent Probe of Molecular Eigenstates. *Chem. Phys. Lett.* **1992**, *197*, 556−561.
(58) Thantu, N.; Weber, P. M. Dependence of Two-Photon Ionization Photoelectron Spectra on Laser Coherence Bandwidth. *Chem. Phys. Lett.* **1992**, *214*, 276−280.
(59) Kuthirummal, N.; Weber, P. M. Rydberg States: Sensitive Probes of Molecular Structure. *Chem. Phys. Lett.* **2003**, *378*, 647−653.
(60) Gosselin, J. L.; Weber, P. M. Rydberg Fingerprint Spectroscopy: A New Spectroscopic Tool with Local and Global Structural Sensitivity. *J. Phys. Chem. A* **2005**, *109*, 4899−2904.
(61) Rudakov, F.; Weber, P. M. Ground State Recovery and Molecular Structure Upon Ultrafast Transition Through Conical Intersections in Cyclic Dienes. *Chem. Phys. Lett.* **2009**, *470*, 187−190.
(62) Clayden, J.; Greeves, N.; Warren, S. *Organic Chemsitry*; Oxford University Press: Oxford, U.K., 2012.
(63) Hine, J. The Principle of Least Motion. Application to Reactions of Resonance-Stabilized Species. *J. Org. Chem.* **1966**, *31*, 1236−1244.
(64) Arruda, B. C.; Sension, R. J. Ultrafast Polyene Dynamics: The Ring Opening of 1,3-Cyclohexadiene Derivatives. *Phys. Chem. Chem. Phys.* **2014**, *16*, 4439−4455.
(65) Beez, M.; Bieri, G.; Brock, H.; Heilbronner, E. The Ionization Potentials of Butadiene, Hexatriene, and their Methyl Derivatives: Evidence for Through Space Interaction Between Double Bond π-Orbitals and Non-Bonded Pseudo-π Orbitals of Methyl Groups? *Helv. Chim. Acta* **1973**, *56*, 1028.
(66) Gavin, R. M., Jr.; Rice, S. A. Spectroscopic Properties of Polyenes. II. The Vacuum Ultraviolet Spectra of Cis- and Trans-1,3,5-Hexatriene. *J. Chem. Phys.* **1974**, *60*, 3231.
(67) Allan, M.; Dannacher, J.; Maier, J. P. Radiative and Fragmentation Decay of the Cations of Trans- and Cis 1,3,5-Hexatriene of All Trans-1,3,5-Heptatriene in the A(π^{-1}) States, Studied by Emission Photoelectron-Photoion Coincidence Spectroscopy. *J. Chem. Phys.* **1980**, *73*, 3114.
(68) Anderson, N. A.; Pullen, S. H.; Walker, L. A.; Shiang, J. J.; Sension, R. J. Ultrafast Polyene Dynamics in Solution: The Conformational Relaxation and Thermalization of Highly Excited *cis*-1,3,5-Hexatriene as a Function of Initial Conformation and Solvent. *J. Phys. Chem. A* **1998**, *102*, 10588−10598.
(69) Ohta, K.; Naitoh, Y.; Tominaga, K.; Hirota, N.; Yoshihara, K. Femtosecond Transient Absorption Studies of *trans*- and *cis*-1,3,5-Hexatriene in Solution. *J. Phys. Chem. A* **1998**, *102*, 35−44.
(70) Harris, D. A.; Orozco, M. B.; Sension, R. J. Solvent Dependent Conformational Relaxation of *cis*-1,3,5-Hexatriene. *J. Phys. Chem. A* **2006**, *110*, 9325−9333.

■ NOTE ADDED AFTER ASAP PUBLICATION

This paper was published ASAP on August 6, 2015, with incorrect Table 1 header and TOC graphic. The corrected version was republished to the Web on August 7, 2015.

DOI: 10.1021/acs.jpca.5b05672
J. Phys. Chem. A 2015, 119, 8832−8845